

Adsorption efficiency, thermodynamics, and kinetics of amino-functionalized mesoporous calcium silicate for the removal of heavy metal ions

Lihua Liu^{a,b,c,d,*}, Jinyan Liu^a, Tong Li^a, Ganggang Yang^a, Anping Tang^{a,b,c}, Yulin Ling^a

^aSchool of Chemistry and Chemical Engineering, Hunan University of Science and Technology, Xiangtan 411201, China, Tel. +86 731 58291625, email: llh213@163.com, liulihualj@sina.com.cn (L. Liu), 870512305@qq.com (J. Liu), 1546044226@qq.com (T. Li), 214909296@qq.com (G. Yang), anpingxt@126.com (A. Tang), lyl931@126.com (Y. Ling)

^bKey Laboratory of Theoretical Organic Chemistry and Function Molecule, Ministry of Education, Xiangtan 411201, China,

^cHunan Province College Key Laboratory of QSAR/QSPR, Xiangtan 411201, China

^dHunan Provincial Key Laboratory of Controllable Preparation and Functional Application of Fine Polymers, Xiangtan 411201, China

Received 28 October 2017; Accepted 1 March 2018

ABSTRACT

Amino-functionalized mesoporous calcium silicate (MCS-NH₂) was synthesized by past-grafting with calcium nitrate tetrahydrate and sodium metasilicate nonahydrate as raw materials, cetyl trimethyl ammonium bromide as the template, and 3-aminopropyltriethoxysilane as the modifying agent. The structure and composition of MCS-NH₂ were characterized, and the adsorption performance and thermodynamic and kinetic characteristics of MCS-NH₂ were investigated using Pb²⁺, Cd²⁺, Cr³⁺, and Cu²⁺. MCS-NH₂ maintained its mesoporous slit-pore structure with a specific surface area of 114.32 m²/g, and pore size was mainly within 4.5–49 nm in the modification. The amount of –NH₂ grafted to MCS-NH₂ was 1.6106 mmol/g. The equilibrium data of Pb²⁺, Cd²⁺, Cr³⁺, and Cu²⁺ adsorbed by MCS-NH₂ fitted the Langmuir and Redlich–Peterson models well but were more suitable for the latter. The maximum adsorption capacities deduced from the Langmuir model were 717.97, 631.43, 628.61, and 366.88 mg/g for Pb²⁺, Cd²⁺, Cu²⁺, and Cr³⁺, respectively. The adsorption processes were endothermic, entropy increasing, and spontaneous. The adsorption of Pb²⁺, Cd²⁺, Cr³⁺, and Cu²⁺ by MCS-NH₂ was rapid and reached equilibrium within 60 min. The adsorption kinetics fitted the pseudo second-order model well, and the adsorption activation energy was 21.0187, 18.1051, 25.9062, and 16.8084 kJ/mol, respectively. The adsorption mechanisms included physical adsorption, chemical adsorption (especially surface complexing adsorption), and ion exchange, among which chemical adsorption was the dominant mechanism. The findings suggest that MCS-NH₂ can be used as an effective sorbent for removing Pb²⁺, Cd²⁺, Cr³⁺, and Cu²⁺ and other related hazardous metal ions from wastewater.

Keywords: Amino-functionalized mesoporous calcium silicate; Heavy metal ion; Adsorption performance; Adsorption thermodynamics and kinetics; Adsorption mechanism

1. Introduction

Heavy metal ions, especially Pb²⁺, Cd²⁺, Cr³⁺, Hg²⁺, Cu²⁺, Ni²⁺, and Mn²⁺, exhibit high toxicity, are non-biodegradable, easily accumulate in organisms, and ultimately lead to cumulative poisoning; they cause serious environmental pollution and pose severe health threats to humans [1]. Many treatment methods have been developed and utilized to remove heavy metal ions from wastewater. Examples

include traditional chemical precipitation [2], chelation–flocculation [3], chemical reduction [4], ferrite method [5], ion exchange [6], ultrafiltration [7,8], electrochemical method [9,10], flotation [11], biological treatment [12], and adsorption method [13]. However, these approaches present practical limitations in the removal of heavy metal ions from wastewater possessing a low concentration or exhibiting complex compositions, such as complexing agents and other auxiliaries. These properties of wastewater do not meet legal limits and entail high treatment costs. Therefore, improved and innovative methods for heavy metal waste-

*Corresponding author.

water treatment are being developed continuously and have elicited increasing research interest [14,15]. Among existing methods, adsorption is the most widely applied to the treatment of heavy metals because of its simple operation, high efficiency, and low costs [16,17].

The effectiveness of heavy metal wastewater treatment by adsorption relies on the performance of the adsorbent used. The performance of adsorbents is mainly determined by the specific surface area of adsorbents, characteristics of the pore structure, and surface functional groups. Specific surface area determines the surface energy and net force field, which play significant roles in physical adsorption. Pore structure characteristics, which include size and distribution, pore shape, and pore regularity, affect adsorption capacity and selectivity. Surface functional groups, which are key factors in chemical and ion exchange adsorption, influence adsorption efficiency, capacity, and selectivity. Many adsorbents, such as natural clayey [18], activated carbons [19], graphene oxide [20], montmorillonite [21], and zeolite [22], have been developed and studied extensively. Nano-sized, and porous adsorption materials have exhibited significant developments in recent years. Typical examples of these materials include PAMAM/CNT nanocomposites [23], mesoporous magnetite (Fe_3O_4) nanospheres [13], thiol-functionalized Fe_3O_4 @metal-organic framework core-shell magnetic microspheres [24], mesoporous carbon nitride functionalized with melamine-based dendrimer amine [25], mesoporous silica (SBA-15, MCM-48, thiol-functionalized mesoporous silica) [26–28], mesoporous zirconium phosphonate hybrid materials [29], ordered macroporous titanium phosphate [30], and ordered mesoporous carbon materials [31]. However, these adsorption materials suffer from complex operations and high costs. They are also difficult to synthesize, and modifying and scaling their production are a challenge. Therefore, new adsorption materials with high adsorption efficiency, easy preparation, low cost, environment-friendly properties, and minimal secondary pollution should be developed.

Calcium silicate, an inorganic silicate material prepared from calcium hydroxide or calcium salt and silicate under certain conditions, has been widely investigated and applied in cement and building trades [32–34]. Mesoporous calcium silicate (MCS) is extensively applied in tissue repair, drug delivery, and molecular recognition due to its excellent bioactivity, biocompatibility, superior bone-forming bioactivity, and sustained drug delivery [35–38]. MCS also possesses a large specific surface area, high porosity, and negative charge strength [39,40]. Its application to water treatment has therefore elicited attention from researchers. However, the application of MCS to wastewater treatment has focused on the removal of phosphorus in wastewater [39,41,42] and on surface water with low nutrient concentrations [43], dibutyl phthalate [44], fluoride recovery [45], and bisphenol A [46]. The application of MCS and its derivatives in heavy metal wastewater treatment has rarely been reported and mainly includes mesoporous calcium-silicate materials (MCSM) [47], ultrathin calcium silicate hydrate nanosheets [48], and chitosan-coated calcium silicate hydrate mesoporous microspheres [49]. Existing studies have investigated the heavy metal adsorption capacity of these materials. However, research on the thermodynamic and kinetic characteristics of these materials in the

adsorption process, such as enthalpy change (ΔH), entropy change (ΔS), Gibbs free energy (ΔG), and activation energy of adsorption (E_a), is rare and inadequate.

The current work presents the synthesis and characteristics of a new amino-functionalized mesoporous calcium silicate (MCS-NH_2) and its performance in Pb^{2+} , Cd^{2+} , Cr^{3+} , and Cu^{2+} adsorption. The study aims to investigate the efficiency of MCS-NH_2 in heavy metal adsorption, ascertain its thermodynamic and kinetic characteristics, obtain the corresponding parameters, and analyze the adsorption mechanism. This work can provide a fundamental basis for the improvement and application of MCS-NH_2 . The results show that MCS-NH_2 possesses extremely high adsorption capacity and can adsorb various heavy metal ions rapidly. Therefore, MCS-NH_2 is an excellent adsorption material for the treatment of heavy metal wastewater.

2. Experimental

2.1. Materials

Calcium nitrate tetrahydrate was purchased from Tianjin Fengchuan Chemical Reagent Technology Co., Ltd. Sodium metasilicate nonahydrate was purchased from Shantou Xilong Chemical Co., Ltd. Cetyl trimethyl ammonium bromide (CTMAB), and toluene were obtained from Sinopharm Group Chemical Reagent Co., Ltd. 3-aminopropyltriethoxysilane (APTES) was purchased from Shanghai Aladdin Biological Technology Co., Ltd. Triethylene tetramine, ethylene diamine tetraacetic acid (EDTA), and anhydrous ethanol were obtained from Tianjin Fuchen Chemical Reagent Factory. Cadmium chloride and chromium sulfate were obtained from Shenyang Xinguang Chemical Factory. Lead nitrate enneahydrate, copper sulfate pentahydrate, hydrochloric acid, nitric acid, and sodium hydroxide were purchased from Tianjin Damao Chemical Reagent Co., Ltd. All reagents were of analytical grade and used as purchased. Deionized water was employed in the experiments.

2.2. Preparation of MCS-NH_2

The synthetic route of MCS-NH_2 is shown in Fig. 1.

For the synthesis procedure, sodium metasilicate nonahydrate (14.21 g) was completely dissolved in 275 mL of distilled water under constant stirring for 1 h. Then, 0.71 g of CTMAB was added gradually to the solution at a mass ratio of $m(\text{CTMAB}):m(\text{Na}_2\text{SiO}_3 \cdot 9\text{H}_2\text{O}) = 0.05:1$. White gel appeared gradually with the addition of CTMAB, and the solution was stirred for 1 h. This mixture was subjected to drop-wise addition of calcium nitrate solution, which was obtained by dissolving 11.81 g of calcium nitrate tetrahydrate in 75 mL of distilled water (at a molar ratio of calcium nitrate tetrahydrate to sodium metasilicate nonahydrate = 1:1). White glue gradually formed with the addition of calcium nitrate tetrahydrate. The intermediate product (MCS) was obtained by filtering after 5 h of reaction, washing for 3–4 times with distilled water, extraction for 24 h with anhydrous ethanol, and drying in a vacuum oven at 50°C for 24 h.

Then, 3.0 g of the MCS was dispersed into 50 mL of toluene solution under constant stirring for 1 h, followed by the drop-wise addition of 5 mL of APTES and reaction for

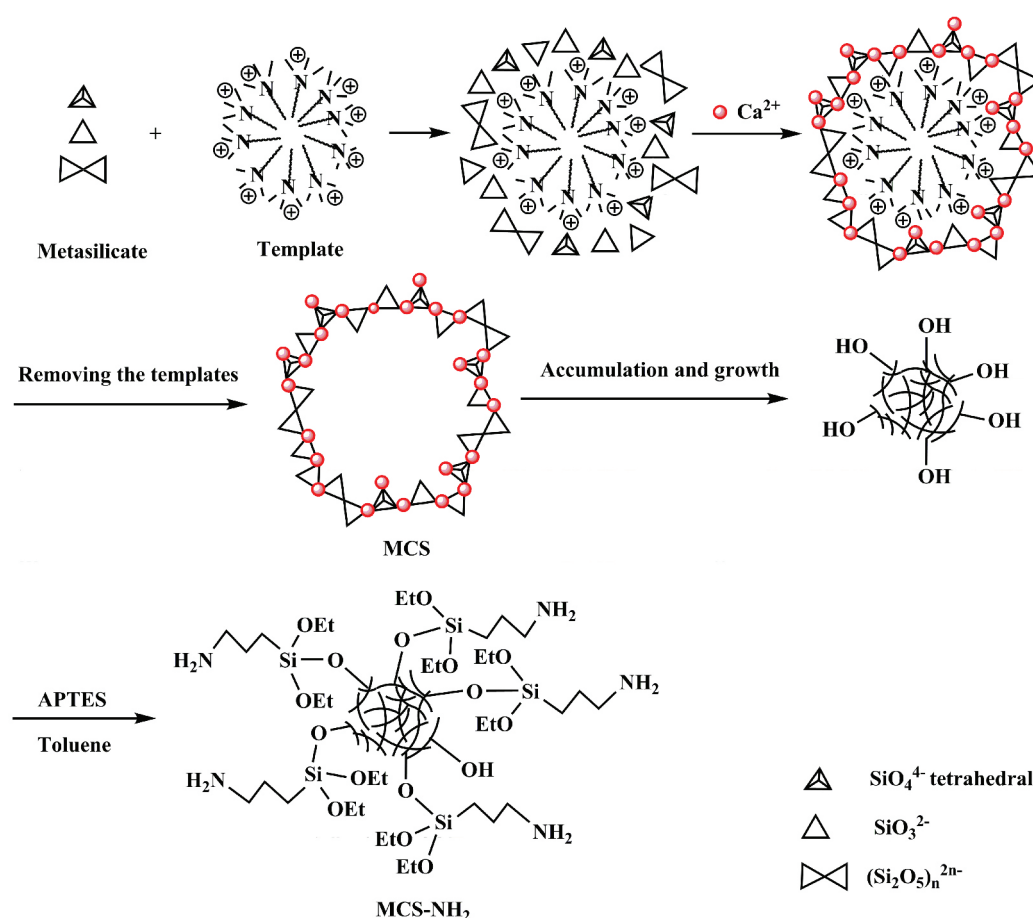


Fig. 1. Synthetic route of MCS-NH₂.

24 h at 120°C. The final product (MCS-NH₂) was obtained by filtering, washing with ethanol and distilled water three times, and drying in a vacuum oven at 40°C for 12 h.

2.3. Adsorption studies

Adsorption studies were conducted to evaluate the adsorption performance of MCS-NH₂ for Pb²⁺, Cd²⁺, Cr³⁺, and Cu²⁺. Simulated heavy metal wastewater samples containing 25, 50, 75, 100, 125, and 150 mg/L of Pb²⁺, Cd²⁺, Cr³⁺, and Cu²⁺ were initially used as test samples, and the synthesized MCS-NH₂ and MCS were used as adsorbents. The particle size distributions of MCS-NH₂ and MCS in water were shown in Table A.1 of the Supplementary Material.

2.3.1. Effect of the initial pH value

The pH values of the 100 mg·L⁻¹ simulated heavy metal wastewater samples were adjusted with 0.1 mol/L of HNO₃ or NaOH solution to 3.5, 4, 4.5, 5, 5.5, 6, 6.5, 7, and 7.5 to evaluate the effect of solution pH on adsorption performance. Adsorption experiments were conducted as follows. First, 50 mL of the simulated heavy metal solution was added to a series of 100 mL conical flasks. Second, 10 mg of MCS-NH₂ was added to each flask, which was placed in a KYC-111-

type thermostatic water bath shaker (Shanghai Fuma Laboratory Equipment Co., Ltd.) to oscillate at a speed of 200 r/min for 10 h at 293 K. Third, the conical flasks were removed from the shaker, and the supernatant solution was separated from the adsorbent via centrifugation for 30 min after standing for 10 min in an Eppendorf 5430 centrifuge (Eppendorf Company, Germany). The residual heavy metal concentration in the supernatant solution was determined using an atomic absorption spectrometer. Adsorption ratio φ and equilibrium adsorption amount q_e were calculated using Eqs. (1) and (2), respectively. Afterward, a φ (q_e)-pH diagram was plotted.

$$\varphi = \frac{(c_0 - c_e)}{c_0} \times 100 \quad (1)$$

$$q_e = \frac{(c_0 - c_e)v}{m} \quad (2)$$

where φ (%) is the adsorption ratio; c_0 and c_e are the initial and equilibrium concentrations (mg/L) of heavy metal ions in the solution, respectively; q_e (mg/g) is the equilibrium adsorption amount of heavy metal ions; v (L) is the solution volume; and m (g) is the adsorbent mass.

2.3.2. Isothermal adsorption experiment

Isothermal adsorption experiments were conducted in accordance with the method and steps in Section 2.3.1. The concentrations of the simulated heavy metal solutions were 25, 50, 75, 100, 125, and 150 mg/L, and the test solution volumes and dosages of MCS-NH₂ were 50 mL and 10 mg, respectively. The adsorption temperatures were 293, 303, 313, and 323 K. Adsorption isotherms at different temperatures were obtained by plotting the equilibrium adsorption amount for a heavy metal ion (q_e) against the equilibrium concentration of the heavy metal ion in solution (c_e) in accordance with the variation in heavy metal ion concentration at pre- and post-adsorption. The experimental data were adjusted to Langmuir, Freundlich, and Redlich–Peterson models (adsorption isotherm models, Supplementary Material). The adsorption thermodynamic parameters were then obtained (adsorption thermodynamic parameters, Supplementary Material).

2.4. Adsorption kinetic experiment

Subsequently, 50 mL aliquots of 150 mg/L of the simulated heavy metal wastewater were individually added to 100 mL conical flasks. Afterward, 10 mg of MCS-NH₂ was added to each flask, which was then placed in a thermostatic water bath shaker under 293 K to oscillate at a speed of 200 rpm for 0–180 min. A conical flask was removed from the shaker at certain intervals, and the supernatant solution was separated from the adsorbent via centrifugation for 30 min after standing for 10 min. The heavy metal concentration in the supernatant solution was determined using an atomic absorption spectrometer, and the adsorption amounts (q_t) at different times were calculated from the results. The adsorption rate constant at 303, 313, and 323 K were determined through the same method. The adsorption rate curve was acquired by plotting q_t against time (t).

The adsorption kinetics in the MCS-NH₂–heavy metal system revealed the heavy metal ion adsorption rate onto MCS-NH₂ and the time required to reach equilibrium. This information is crucial for a thorough understanding of the adsorption process and adsorbent performance. The experimental adsorption kinetic data were analyzed by applying pseudo first-order and pseudo second-order kinetic models, and the adsorption kinetic parameters and adsorption activation energy were obtained (adsorption kinetic models and adsorption activation energy, Supplementary Material).

2.5. Regeneration investigation

MCS-NH₂ (30 mg) was added to a 250 mL conical flask with 150 mL of 100 mg/L Pb²⁺, Cd²⁺, Cr³⁺, and Cu²⁺ solution. Then, the conical flask was sealed and placed in a thermostatic shaker at 200 rpm for 10 h at 293 K. The supernatant solution was separated from the adsorbent by filtering after standing for 20 min, and the heavy metal ion concentrations in the filtrate were measured. The recovered adsorbents were added to 100 mL of 0.1 mol/L of eluent (triethylenetetramine, EDTA, and HCl solutions) to regenerate for 6 h. The regenerated adsorbents were obtained by filtering, washing with deionized water three times, and then drying to a constant weight in a vacuum oven at 60°C. Afterward,

the regenerated MCS-NH₂ was used for repeated adsorption experiments to measure the variation in adsorption properties for heavy metal ions.

2.6. Adsorption mechanism investigation

To determine if the ion exchange mechanism occurs in MCS-NH₂ adsorption for heavy metal ions, the concentration of Ca²⁺ released from the adsorption procedure was determined simultaneously with the determination of the residue heavy metal ion of the adsorption solution.

2.7. Analytical method

X-ray diffraction (XRD) patterns were obtained with a D8 Advance X-ray diffractometer (Bruker Co., Germany) and used to identify the phase structures of the samples. Fourier transform infrared (FT-IR) spectroscopy was performed with the KBr pellet method on a Spectrum One (B) FT-IR spectrophotometer (Perkin Elmer Co., America) between 400 and 4000 cm⁻¹. The elemental nitrogen content was measured with a Vario EL III elementary analysis instrument (Elementar Co., Germany) at 950°C. The N₂ adsorption–desorption isotherms were determined with a specific surface area and pore volume analyzer (BEL SORP II, BELSOKP, Japan) at 77 K, and the specific surface area was calculated through Brunauer–Emmett–Teller (BET) and Barrett–Joyner–Halenda methods. The morphologies of the samples were tested via field-emission scanning electron microscopy (SEM; S-4800, Hitachi Co., Japan), and energy spectrum analysis was conducted with a field-emission transmission electron microscope (Tecna G2 F20, FEI, America). Thermogravimetry–differential thermal analysis (TG-DTA) was conducted with an STA409PC/4/H thermal analyzer (NETZSCH, Germany). Heavy metal ion and Ca²⁺ concentrations were measured using an A-Analyst 300 atomic absorption spectrometer (Perkin Elmer Co., America).

3. Results and discussion

3.1. Characterization of MCS-NH₂

Figs. 2–7 show the XRD, FT-IR, EDX, DTA-TG, SEM, TEM, and BET images of MCS-NH₂. The corresponding characterization results of MCS are also presented to facilitate a comparison.

As shown in Fig. 2, the XRD pattern of MCS-NH₂ is basically similar to that of MCS. Strong diffraction peaks are present at 2 theta = 29.5°, and the diffraction peaks elsewhere are diffused, which signify the low crystallinity of MCS-NH₂ and MCS. Contrary to the results of Shaw et al. [50] indicating that crystalline calcium silicate hydrates have a wide range of structures with various Ca/Si molar ratios, the current work revealed that MCS exhibits low crystallinity despite synthesis using a Ca/Si molar ratio of 1:1. Relative to the standard JCPDS card, MCS-NH₂ involves CaSi₂O₅ (PDF# 51-0092), Ca₂SiO₄·H₂O (PDF# 29-0373), and Ca₂SiO₄ phases (PDF# 49-1672), similar to MCS. These results indicate that amino modification exerts no effect on the structure of MCS due to the high stability of the material.

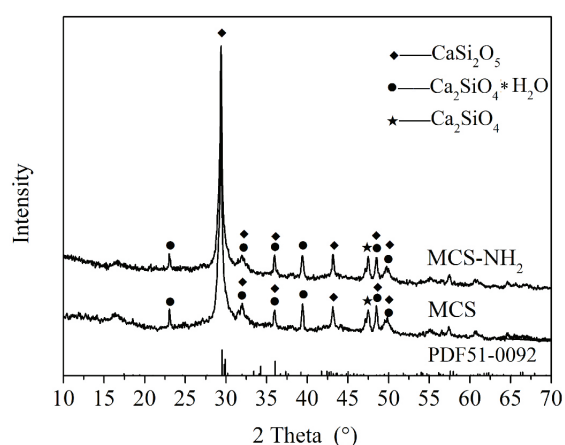
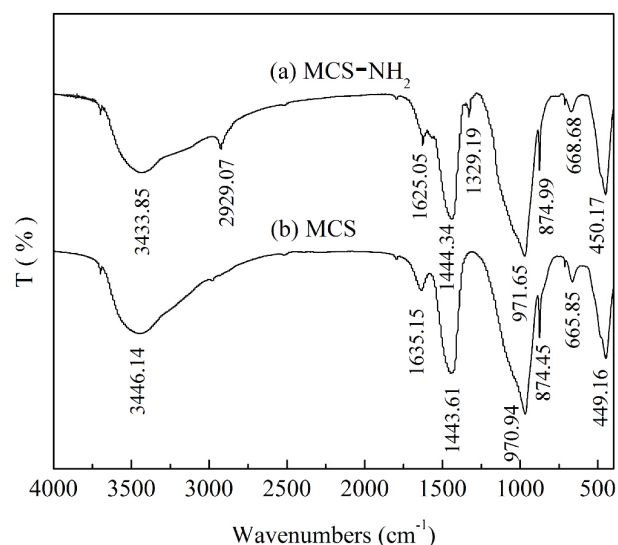
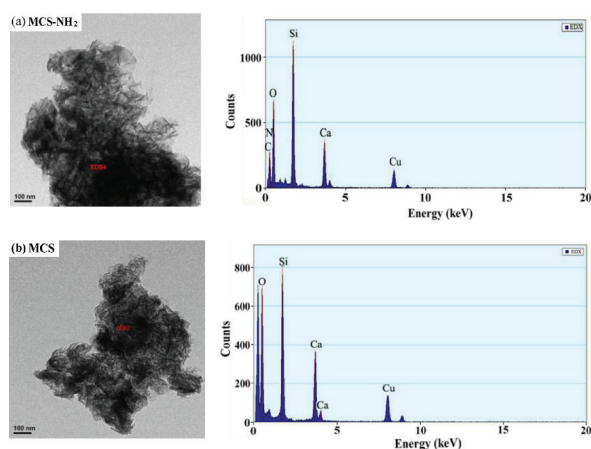
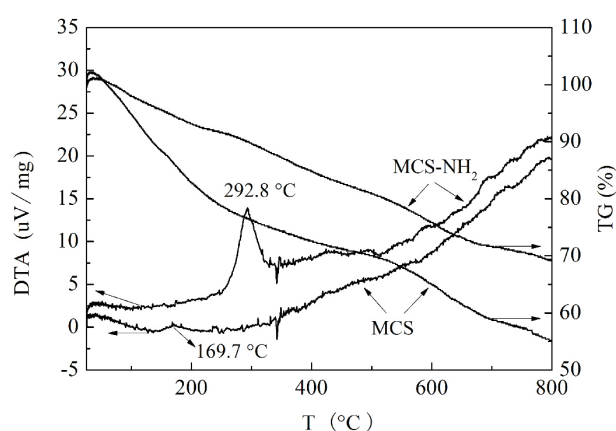
Fig. 2. XRD patterns of MCS-NH₂ and MCS.Fig. 3. FT-IR spectra of MCS-NH₂ (a) and MCS (b).Fig. 4. Energy spectra of MCS-NH₂ (a) and MCS (b).Fig. 5. DTA-TG curves of MCS-NH₂ and MCS.

Fig. 3 shows that after amino functionalization, the main IR absorption peaks are basically the same, but MCS-NH₂ presents absorption peaks that differ from those of MCS. The bands at 3433.85 cm⁻¹ in Fig. 3(a) can be ascribed to the stretching vibration of O–H of –OH and N–H of –NH₂ on the surface of MCS-NH₂, whereas the bands at approximately 1625 cm⁻¹ can be attributed to the bending vibration of O–H of the absorbed water and the bending vibration of N–H of –NH₂ [51] that leads to red shifting [Fig. 3(b)]. The bands at approximately 1440 cm⁻¹ are due to SiO₃²⁻ of calcium silicate, and the bands at approximately 970 and 875 cm⁻¹ are attributed to the Si–O–Si symmetric stretching vibration of the skeleton and the characteristic absorption peak of Si–O tetrahedron [32,52], respectively. In addition, the bands at approximately 665 and 450 cm⁻¹ are ascribed to the stretching vibration of O–Si–O and the bending vibration of Si–O–Si [32,33], respectively. Compared with Fig. 3b, Fig. 3a shows the presence of two weak bands after modification with APTES. Asymmetric stretching and bending vibrations of –CH₂– are observed at 2929.07 and 1329.19 cm⁻¹, respectively; the strength of –OH stretching and bending vibration peaks at 3433.85 and 1625.05 cm⁻¹ are weakened due to the replacement of –OH on the surface of MCS by –NH₂ after silylation. These results indicate the successful modification of the group –SiCH₂CH₂CH₂NH₂ of APTES on MCS-NH₂, as verified further via energy spectrum and TG-DTA analyses.

Fig. 4 and Table A.2 of the Supplementary Material indicate the appearance of obvious adsorption peaks of C and N in the energy spectrum analysis diagram of MCS-NH₂; their mass percentages are 29.684% and 1.988%, respectively. The same phenomenon is not observed in MCS. These results reveal the successful modification of the group –SiCH₂CH₂CH₂NH₂ onto MCS, as verified by the FT-IR analysis results. The nitrogen content of MCS-NH₂ was 2.256%, as determined with a Vario EL III elementary analysis instrument. The amount of the –NH₂ group grafted was calculated to be 1.6106 mmol/g.

Fig. 5 reveals the presence of an exothermic peak, the weight loss of which is approximately 4.3% and observed at 292.8 °C in the TG-DTA curve of MCS-NH₂. No peak exists in the corresponding position in the TG-DTA curve of MCS, although a weak exothermic peak is noted at 169.7 °C

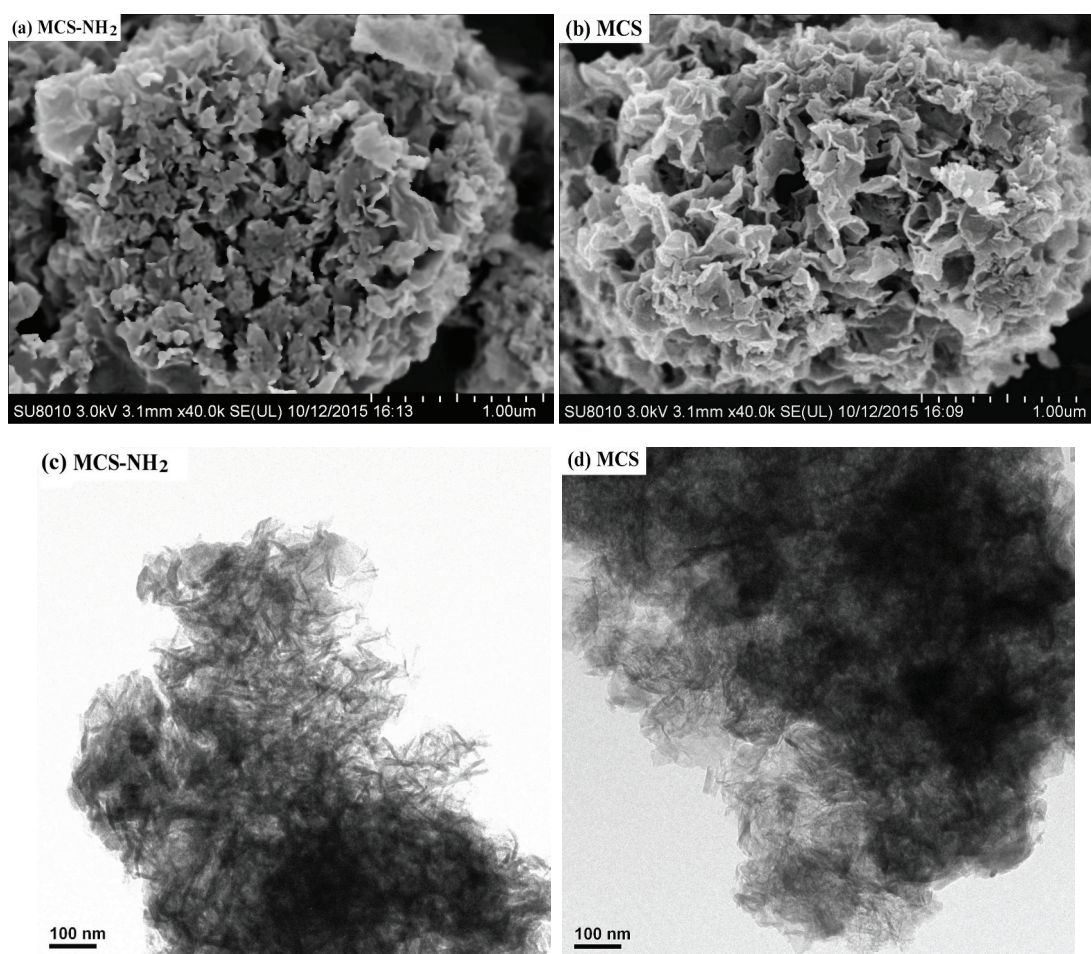


Fig. 6. SEM and TEM images of MCS-NH₂ and MCS.

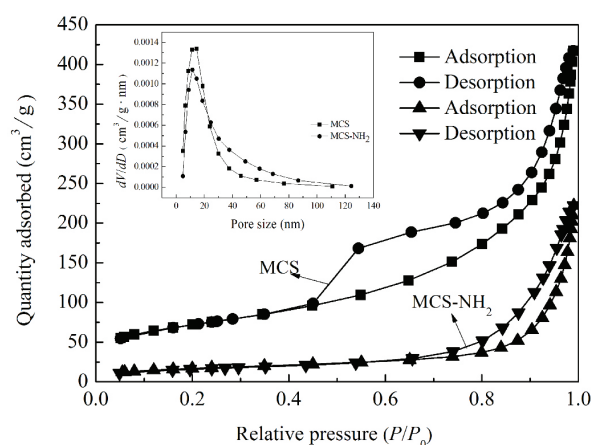


Fig. 7. Nitrogen adsorption-desorption isotherms and pore size distribution curves of MCS-NH₂ and MCS.

on the basis of the DTA curve of MCS. This result is possibly due to the minimal amounts of absorbed impurities and CTMAB that remained after washing and extraction during the preparation of MCS. The absorbed impurities

are released during the heating process, leading to a weight loss of approximately 11% between 25°C and 145°C. When the temperature increases to 169.7°C, the residual CTMAB begins to decompose, leading to a weak exothermic peak. For MCS-NH₂, the remaining impurities and CTMAB are completely removed after immersion in toluene solution for 25 h and washing by ethanol and distilled water during the preparation of MCS-NH₂. Therefore, no exothermic peak appears. The exothermic peak at 292.8°C may be due to the oxidation-decomposition of the -SiCH₂CH₂CH₂NH₂ group modified on the calcium silicate surface. The weight loss between 340°C and 800°C can be attributed to the condensation-dehydration of Si-OH on the pore wall of calcium silicate. These results further prove the successful modification of the -SiCH₂CH₂CH₂NH₂ group on calcium silicate.

Figs. 6a and 6b indicate that the slit-like channels of MCS-NH₂ and MCS are made up of slices with various shapes, and their surfaces are uneven. MCS exhibits a flower-like morphology. Although the structure of MCS-NH₂ is similar to that of MCS (Fig. 6b), the channels of the former are filled with small granules. This characteristic is due to the number of slices that break during amino functionalization. The TEM images (Figs. 6c and 6d) show that MCS-NH₂ and MCS are composed of slices, and their intermediate channels are distributed intensively. Hence, the structure of

MCS can be maintained because of its high stability even in cases where the channels are blocked by small granules during modification. These abundant channels and uneven surface facilitate the adsorption of heavy metal ions.

Fig. 7 shows the nitrogen adsorption–desorption isotherms and pore size distribution curves of MCS-NH₂ and MCS. The specific surface areas of MCS-NH₂ and MCS were calculated using the BET method, and their pore sizes were calculated from the desorption branch of the isotherm with the Barrett–Joyner–Halenda method. The results are shown in Table 1. The isotherms of MCS-NH₂ and MCS belong to type V with a hysteresis loop of the H3 type according to IUPAC classifications. The pore size distributions of MCS-NH₂ and MCS are relatively centralized and range from 4.5–49 nm and 4–50 nm, respectively. Therefore, MCS-NH₂ and MCS are mesoporous. The results shown in Table 1 indicate that the specific surface area and pore size of the modified MCS-NH₂ decrease by 43.81 m²/g and 1 nm, respectively, relative to those of the unmodified MCS. These low values are due to the successful modification of the –SiCH₂CH₂CH₂NH₂ group on MCS-NH₂ and the damage of the calcium silicate slices that filled the channels of calcium silicate during modification. These conditions lead to the decrease in the specific surface area and pore size.

3.2. Effect of pH

Fig. 8 shows the change in the adsorption ratios of Pb²⁺, Cd²⁺, Cr³⁺, and Cu²⁺ with the pH values. When the solution pH is 5.0–7.5, the adsorption ratios of MCS-NH₂ for Pb²⁺, Cd²⁺, Cr³⁺, and Cu²⁺ are high. When the solution pH is 3.50, the adsorption ratios are low. At a pH of less than 5, the

Table 1
Specific surface area and pore size of MCS-NH₂ and MCS

Sample	S_{BET} (m ² /g)	D_{BJH} (nm)
MCS-NH ₂	114.32	18
MCS	158.13	19

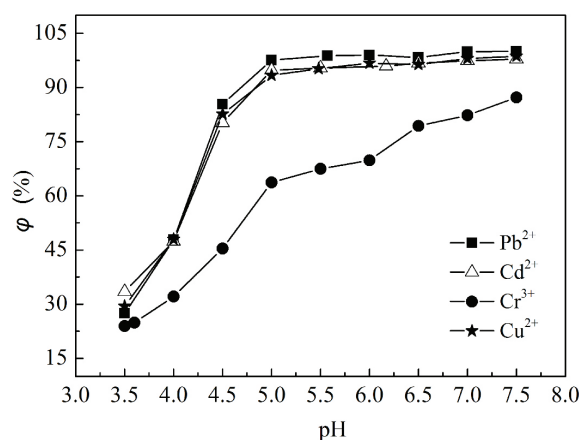


Fig. 8. Effect of initial pH value of the simulated heavy metal solution on adsorption ratio.

adsorption ratios increase rapidly with increasing pH. When pH reaches 5, the adsorption ratios of MCS-NH₂ for Pb²⁺, Cd²⁺, Cr³⁺, and Cu²⁺ are 97.57%, 94.78%, 63.73%, and 93.35%, respectively. The adsorption ratios for Pb²⁺, Cd²⁺, and Cu²⁺ begin to stabilize with small changes, whereas those for Cr³⁺ begin to increase significantly after stabilizing at a pH of 5.0–6.0. This result is attributed to the appearance of precipitates at pH > 6.0, thereby increasing the adsorption ratios. When the solution pH is not adjusted, the initial pH values of 100 mg·L⁻¹ Pb²⁺, Cd²⁺, Cr³⁺, and Cu²⁺ solution are 5.51, 6.17, 3.60, and 5.48, respectively, and the adsorption ratios are 98.79%, 95.91%, 24.87%, and 95.21%, respectively. The adsorption ratios of Cr³⁺ at the investigated pH values are all low, especially at the initial pH = 3.60. Therefore, the pH of the Cr³⁺ solution must be adjusted to above 5.0. However, precipitates begin to form at pH = 5.5. Thus, the pH value of the Cr³⁺ solution is suitable to be adjusted to 5.0–5.5, and the pH values of the three other heavy metal ions need not be adjusted.

3.3. Adsorption isotherm and thermodynamics of MCS-NH₂ for heavy metal ions

3.3.1. Adsorption isotherm

The adsorption isotherms of MCS-NH₂ for Pb²⁺, Cd²⁺, Cr³⁺, and Cu²⁺ are depicted in Fig. 9. The pH values of the simulated Cd²⁺, Cu²⁺, and Pb²⁺ solutions were not adjusted, and that of Cr³⁺ was adjusted in the range of 5.0–5.5 (Table A.3, Supplementary Material).

Fig. 9 shows that the equilibrium adsorption capacities (q_e) of MCS-NH₂ for Pb²⁺, Cd²⁺, Cr³⁺, and Cu²⁺ increase rapidly with the solution concentration when the heavy metal solution concentrations are less than 100 mg/L (fourth experimental point) at the same temperature. Beyond 100 mg/L, the equilibrium adsorption capacities increase only slightly, even with the continuous increase in heavy metal solution concentration. The adsorption isotherms of MCS-NH₂ for Pb²⁺, Cd²⁺, Cr³⁺, and Cu²⁺ also increase as the temperature increases. The results indicate that the adsorption amounts increase with temperature, and adsorption is an endothermic reaction that mainly belongs to chemical adsorption.

The data in Fig. 9 are fitted using Langmuir, Freundlich, and Redlich–Peterson models, and the results are shown in Table A.4 of the Supplementary Material. The correlation coefficient fitted by the Redlich–Peterson model is the highest, followed by those fitted by the Langmuir and Freundlich models. The Redlich–Peterson and Langmuir models can fit the experimental data well. However, the Redlich–Peterson model is more accurate than the Langmuir model because it combines the success of the Langmuir and Freundlich models and is not bounded by the ideal monolayer assumption of the Langmuir model (adsorption isotherm models, Supplementary Material). As such, the Redlich–Peterson model is especially suitable for describing the uneven surfaces of physical and chemical adsorption. In addition to chemical adsorption, physical adsorption also exists. Under the Langmuir adsorption model, the maximum adsorption capacities of MCS-NH₂ for Pb²⁺, Cd²⁺, Cr³⁺, and Cu²⁺ at 293 K are 717.97, 631.43, 366.88, and 628.61 mg/g, respectively. These values are much higher than those of common adsor-

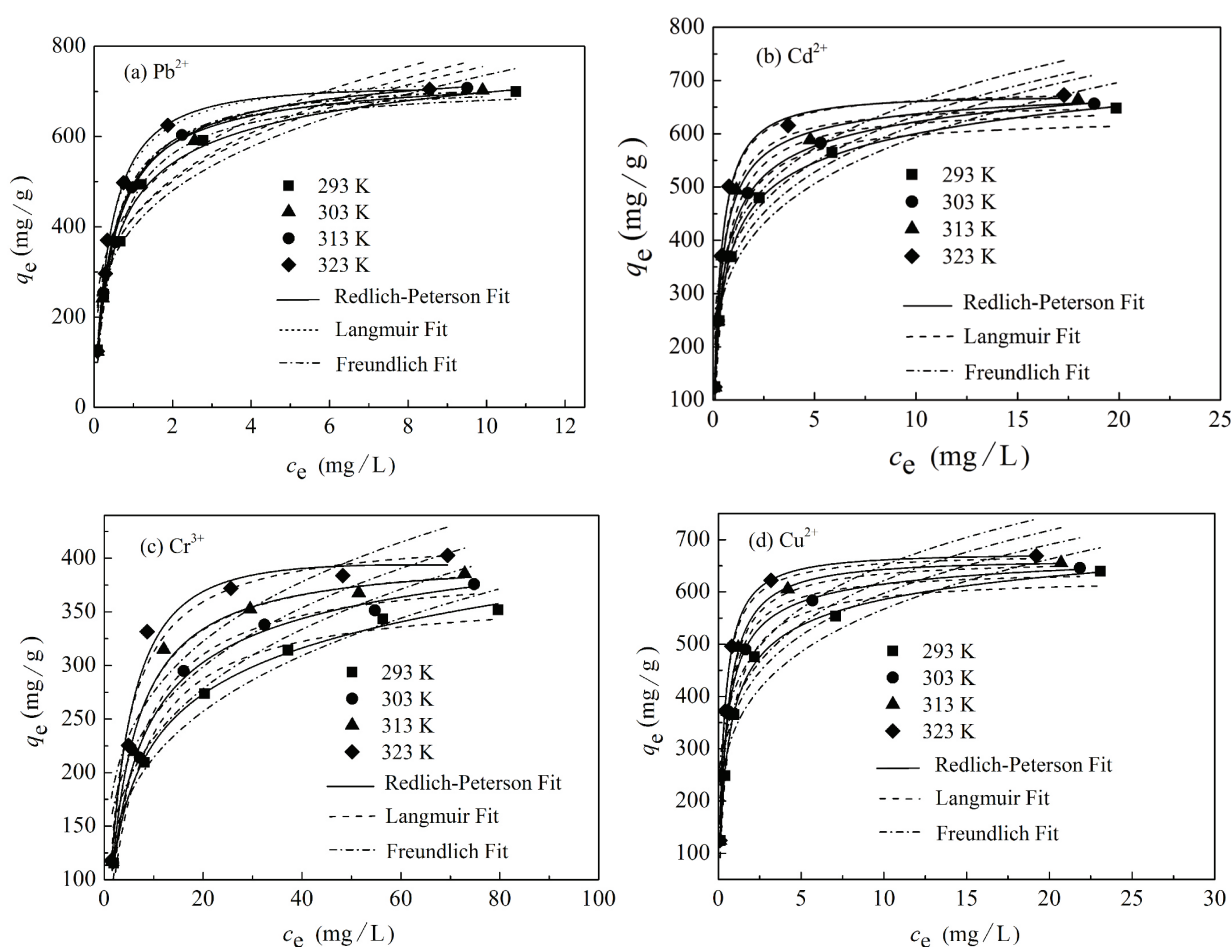


Fig. 9. Adsorption isotherms of MCS-NH₂ for Pb²⁺ (a), Cd²⁺ (b), Cr³⁺ (c), and Cu²⁺ (d).

bents reported in literature and those of MCS (Table 2). The order of adsorption capacities for Pb²⁺, Cd²⁺, Cr³⁺, and Cu²⁺ is Pb²⁺ > Cd²⁺ > Cu²⁺ > Cr³⁺ in mg/g and Cu²⁺ > Cr³⁺ > Cd²⁺ > Pb²⁺ in mmol/g.

3.3.2. Adsorption thermodynamic characteristics

The heavy metal ion distribution coefficients (K_d) at adsorption equilibrium and at different temperatures were calculated according to Eq. (A.4) of the Supplementary Material to explore the adsorption thermodynamic characteristics of MCS-NH₂ for Pb²⁺, Cd²⁺, Cr³⁺, and Cu²⁺. The relationship curves between the logarithm $\ln K_d$ and the reciprocal of temperature ($1/T$) are plotted in Fig. 10. Given the intercept and slope of the fitted lines, the adsorption thermodynamic parameters, such as ΔS , ΔH , and ΔG , were calculated according to Eqs. (A.5) and (A.6) of the Supplementary Material. The results are shown in Table 3.

Table 3 shows that the ΔH and ΔS of the adsorption process of MCS-NH₂ for the heavy metal ions are all above zero, and ΔG is less than zero. Hence, the adsorption processes are spontaneous endothermic processes with increasing entropy. Apart from the large specific

surface area and abundant pore canals, abundant active groups, such as –OH and –O–, are present on the surface of MCS-NH₂ [41]; in particular, 1.6106 mmol/g –NH₂ is observed. The adsorption of MCS-NH₂ for the heavy metal ions primarily involves chemical adsorption caused by the coordination effect of active groups of –OH, –O–, and –NH₂ with heavy metal ions. Therefore, the process requires the absorption of a certain amount of energy to overcome the activation energy and exhibit heat absorption. Chemical adsorption only contributes partly to the adsorption; thus, the heat absorption amount is small. The increase in the adsorption entropy of MCS-NH₂ for Pb²⁺, Cd²⁺, Cr³⁺, and Cu²⁺ may be due to the fact that the heavy metal ions in the aqueous solution are solvated. MCS-NH₂ may have adsorbed a certain amount of solvent molecules in the preparation process. When the heavy metal ions are adsorbed onto the MCS-NH₂ surface, they are constrained to the surface, leading to decreased entropy of the adsorption process. The solvent molecules adsorbed onto the adsorbent surface and the solvent layer are partly released from the MCS-NH₂ surface and the solvent layer of the heavy metal ions, thereby increasing the entropy. The entropy decrement from the heavy metal ions constrained to the surface of MCS-NH₂ is lower than the entropy incre-

Table 2
Comparison of adsorption capacities of MCS-NH₂ toward heavy metal ions with those reported in the literature

Adsorbent	Adsorption capacity (mg/g)				References
	Cd ²⁺	Cu ²⁺	Pb ²⁺	Cr ³⁺	
Amino functionalized magnetic graphenes composite material	27.83	–	27.95	–	[1]
Peanut husk	11.36	–	27.03	–	[12]
Mesoporous magnetite (Fe ₃ O ₄) nanospheres	–	–	19.0	–	[13]
Al ₂ O ₃ -pillared layered MnO ₂	–	–	29.2	–	[14]
Palygorskite	0.6971	2.356	–	–	[17]
Sepiolite	5.234	8.683	–	–	
Natural clayey adsorbent	–	–	86.4	–	[18]
Granular activated carbon	–	–	47.2	–	[19]
Na(I)-montmorillonite	22.93	9.66	54.28	–	[21]
Ca(II)-montmorillonite	17.87	6.61	34.19	–	
Thiol-functionalized Fe ₃ O ₄ @metal-organic framework core-shell magnetic microspheres	–	–	215.05	–	[24]
Mesoporous carbon nitride functionalized with melamine-based dendrimer amine	–	199.75	196.34	–	[25]
Modified magnetic mesoporous silica MCM-48	114.08	125.80	127.24	–	[27]
Mesoporous Zirconium Phosphonate Hybrid Material	312.0	327.1	485.3	–	[29]
Ordered Macroporous Titanium Phosphonate Materials	7.19	9.97	9.32	–	[30]
Surface Functionalization of Ordered Mesoporous Carbon (FDU-15)	79.81	69.90	223.78	–	[31]
Chitosan-coated mesoporous microspheres of calcium silicate hydrate	578	425	796	–	[49]
Dithiocarbamate carbon nanotubes	202.43	101.52	–	–	[53]
Ammonium persulfate oxidized activated carbon fibers	–	–	559.44	–	[54]
Graphene oxide membranes	91.05	76.89	–	–	[55]
Chitosan/Sulfhydrylfunctionalized graphene oxide composites	177	425	447	–	[56]
MCS* (293 K)	436.14	391.82	451.49	272.26	This work
MCS-NH ₂ (293 K)	631.43	628.61	717.97	366.88	This work

* The conditions of MCS adsorbing Pb²⁺, Cd²⁺, Cr³⁺ and Cu²⁺ are same as those of MCS-NH₂.

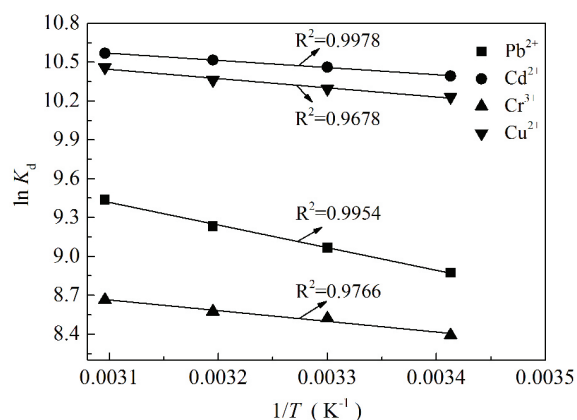


Fig. 10. $\ln K_d$ vs. $1/T$ for Pb²⁺, Cd²⁺, Cr³⁺, and Cu²⁺ adsorption onto MCS-NH₂.

ment from the release of solvent molecules. Consequently, entropy increases.

3.4. Adsorption kinetic characteristics

Fig. 11 shows the change in the adsorption amount (q_t) of heavy metal ions with time t at different temperatures. The kinetic fitting parameters are shown in Table A.5 of the Supplementary Material.

The adsorptions of MCS-NH₂ for Pb²⁺, Cd²⁺, Cr³⁺, and Cu²⁺ are all rapid, and the adsorption amounts (q_t) quickly increase within 10 min after adding MCS-NH₂; the periods before equilibrium is attained are all within 60 min, i.e., 40, 30, 40, and 60 min, respectively. Fig. 11 and Table A.5 of the Supplementary Material show that the adsorption capacities of MCS-NH₂ for Pb²⁺, Cd²⁺, Cr³⁺, and Cu²⁺ fit the pseudo second-order kinetic model well. The fitted values are also

Table 3
Thermodynamic parameters of MCS-NH₂ adsorption for Pb²⁺, Cd²⁺, Cr³⁺ and Cu²⁺

Metal ion	R ²	ΔH kJ/mol	ΔS (J/mol·K)	ΔG (kJ/mol)			
				293 K	303 K	313 K	323 K
Pb ²⁺	0.9954	5.9360	112.3920	-26.9949	-28.1188	-29.2427	-30.3666
Cd ²⁺	0.9978	4.5940	102.1059	-25.3230	-26.3441	-27.3651	-28.3862
Cr ³⁺	0.9678	6.8653	93.3080	-20.4739	-21.4070	-22.3401	-23.2732
Cu ²⁺	0.9766	5.9153	105.1663	-24.8984	-25.9501	-27.0017	-28.0534

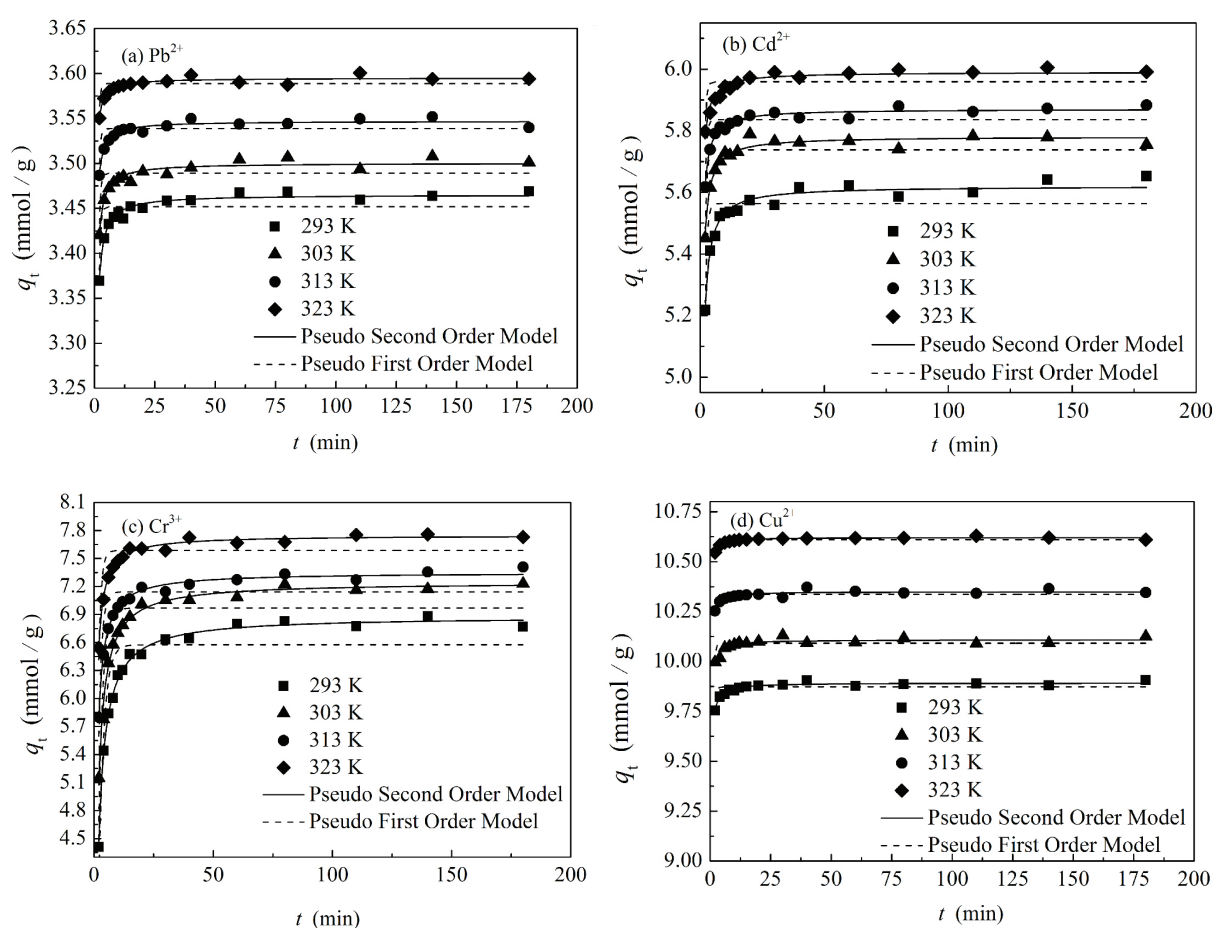


Fig. 11. Change in the adsorption amount (q_t) with time (t) at different temperatures: (a) Pb²⁺; (b) Cd²⁺; (c) Cr³⁺; (d) Cu²⁺.

close to the experimental values (q_{ed}). The logarithm of the secondary adsorption rate constant (Table A.5, Supplementary Material) $\ln k$ is plotted against the reciprocal of temperature $1/T$ (Fig. 12).

A good correlation exists between $\ln k$ at different temperatures and $1/T$ (Fig. 12). The activation energy of the adsorption process was calculated from the slope of the fitted curve on the basis of Eq. (A.9) of the Supplementary Material. The results are shown in Table A.6 of the Supplementary Material. The order of adsorption activation energy is Cr³⁺ (25.9062 kJ/mol) > Pb²⁺ (21.0187 kJ/mol) > Cd²⁺ (18.1051 kJ/mol) > Cu²⁺ (16.8084 kJ/mol).

3.5. Regeneration of MCS-NH₂

MCS-NH₂ can be dissolved by using 0.1 mol/L of EDTA or HCl solutions as the eluent. Thus, such solutions cannot be used as eluents. Table 4 presents the regeneration of the MCS-NH₂-adsorbed Pb²⁺, Cd²⁺, Cr³⁺, and Cu²⁺ by using 0.1 mol/L of triethylene tetramine.

Table 4 shows that 0.1 mol/L of triethylene tetramine can regenerate MCS-NH₂ well. After the first elution regeneration, the decreasing percentages of the equilibrium adsorption values become significant at 15.06%, 13.19%, 21.46%, and 16.51% for Pb²⁺, Cd²⁺, Cr³⁺, and Cu²⁺, respec-

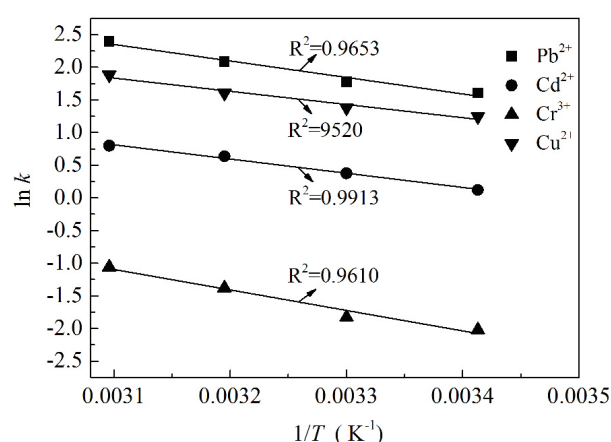


Fig. 12. $\ln k$ vs. $1/T$ for Pb^{2+} , Cd^{2+} , Cr^{3+} , and Cu^{2+} adsorption onto MCS-NH_2 .

Table 4
Regeneration of MCS-NH_2 from Pb^{2+} , Cd^{2+} , Cr^{3+} and Cu^{2+} adsorption

Metal ion	Items	Regeneration times		
		0	1	2
Pb^{2+}	Equilibrium adsorption value q_e (mmol/g)	2.39	2.03	1.64
	Decreasing percent (%)		15.06	31.38
Cd^{2+}	Equilibrium adsorption value q_e (mmol/g)	4.32	3.75	3.06
	Decreasing percent (%)		13.19	29.17
Cr^{3+}	Equilibrium adsorption value q_e (mmol/g)	6.15	4.83	3.57
	Decreasing percent (%)		21.46	41.95
Cu^{2+}	Equilibrium adsorption value q_e (mmol/g)	7.57	6.32	5.17
	Decreasing percent (%)		16.51	31.70

tively; these values increase to 31.38%, 29.17%, 41.95%, and 31.70%, respectively, after the second elution regeneration. Therefore, continuous elution and regeneration are of little value. These results indicate that after adsorbing Pb^{2+} , Cd^{2+} , Cr^{3+} , and Cu^{2+} , the adsorbent exhibits irreversible changes. The decreasing percentage for Cr^{3+} reaches 41.95%, indicating the poor elution effect of triethylene tetramine. The elution of heavy metals from MCS-NH_2 mainly depends on the strong coordination capability or the ion exchange capacity of the eluent to contest heavy metal ions adsorbed from the adsorbent to the solution to realize desorption. As a result of the adsorption of Cr^{3+} at a pH above 5, the dominant species of Cr^{3+} is tetrameric $\text{Cr}_4(\text{OH})_9^{3+}$ [57], which is difficult to coordinate with triethylene tetramine.

3.6. Adsorption mechanism

Previous research has indicated that porous calcium silicate, especially jennite, tobermorite, and amorphous

calcium silicate, easily releases Ca^{2+} in aqueous solutions [41,42,45], and they adsorb metal ions mainly on the basis of the Ca^{2+} -ion exchange mechanism [36,58]. To identify the problem, we determined the Ca^{2+} concentration in the adsorption solution (tested solution concentration: 100 mg/L, 50 mL; MCS-NH_2 : 10 mg; temperature: 293 K). The results are shown in Table 5.

The amount of released Ca^{2+} is much less than the adsorption amount of heavy metals, indicating that the adsorption of MCS-NH_2 for heavy metals through ion exchange with Ca^{2+} is only a small fraction and that the main adsorption mechanism is not ion exchange. This result is different from the results of 76.7% Co(II) removed by MCSM by using the ion exchange mechanism [47] and 50% Ca^{2+} in tobermorite irreversibly exchanged by Co^{2+} and Ni^{2+} [55]. The reasons may be as follows. (1) The main phases of MCS-NH_2 in this study are CaSi_2O_5 and $\text{Ca}_2\text{SiO}_4 \cdot \text{H}_2\text{O}$ (Fig. 2), which are different from those of the metastable state of tobermorite [32,47] and calcite [32], with the former being more stable than the latter, especially in acidic solutions. (2) Research has shown that a large specific surface area equates to a rapid release of Ca^{2+} [42]. The results show that the specific surface area of MCS-NH_2 (114.32 m^2/g) is much lower than that of MCSM (733 m^2/g). Thus, the amount of Ca^{2+} released from MCS-NH_2 is low. (3) MCS-NH_2 is modified by APTES, which is beneficial to the increase in stability. (4) The adsorption of Co(II) is carried out at $\text{pH} = 2$, whereas calcite and tobermorite are unstable at this pH. Obvious dissolution of the adsorbent is observed when the initial pH of the solution is below 3.5. As indicated by the elution regeneration results, most of the adsorbed heavy metal ions (approximately 80%) can be eluted easily. If most heavy metal ions are adsorbed via ion exchange with Ca^{2+} , then they become difficult to elute with 0.1 mol/L of triethylene tetramine because of the absence of exchangeable cation with heavy metal ions in the eluent. Therefore, ion exchange is not the main adsorption mechanism in our research.

On the basis of the aforementioned discussion, we propose the following for the adsorption mechanism of MCS-NH_2 for heavy metal ions.

1. Physical adsorption results from a large specific surface area and net force field originating from the polar surface and edge. The hydrated heavy metal ions diffuse from the bulk of the solution to the near surface of MCS-NH_2 . Then, partially hydrated molecules are released and adsorbed on the surface through van der Waals' force and polar force from the net force field. Consequently, physical adsorp-

Table 5
Released amount of Ca^{2+} from MCS-NH_2 after adsorption of heavy metal ions

Adsorbed heavy metal	Pb^{2+}	Cd^{2+}	Cr^{3+}	Cu^{2+}
Adsorption amount of heavy metal (mmol)	0.0239	0.0432	0.0615	0.0757
Released Ca^{2+} amount (mmol)	0.0041	0.0079	0.0069	0.0144

tion is produced, and the entropy of the process increases accordingly.

- Chemical adsorption results from the surface-complexing reaction of active groups of $-O^-$ and $-OH$, especially $-NH_2$ modified on $MCS-NH_2$, with heavy metal ions diffusing to the near surface and releasing hydrated molecules. The result is an increase in entropy. In the current research, the abundance of active groups of $MCS-NH_2$ leads to the dominance of chemical adsorption.
- Ion exchange results from Ca^{2+} on the surface and edge of slices of $MCS-NH_2$ with heavy metal ions. As a result of the heterogeneous equilibrium of ions of the indissoluble calcium silicate, a certain amount of Ca^{2+} exists near the interface of $MCS-NH_2$ /water. When the heavy metal ion diffuses to the interface, it has potential to replace Ca^{2+} into the structure of $MCS-NH_2$ [Formula (3)], thereby producing ion exchange. Only the heavy metal ions that can react with silicate to form M^{n+} -silicate with small solubility products can exchange with Ca^{2+} . Therefore, Ca^{2+} in $MCS-NH_2$ and heavy metal ions with unmatched scales cannot lead to ion exchange adsorption.



The proposed adsorption mechanism model is shown in Fig. 13.

4. Conclusions

- Amino-functionalized $MCS-NH_2$ was successfully synthesized by past-grafting using calcium nitrate tetrahydrate and sodium metasilicate nonahydrate as raw materials, CTMAB as the template, and

APTES as the modifying agent. $MCS-NH_2$ showed slit-like channels and retained its stable mesoporous structure during the modification process. The adsorption-desorption isotherms belonged to type V with a hysteresis loop of H3 type. The specific surface area was $114.32 \text{ m}^2/\text{g}$, and the pore size ranged from $4.5\text{--}49 \text{ nm}$. These values decreased by $43.81 \text{ m}^2/\text{g}$ and 1 nm relative to those of MCS . The amount of the $-NH_2$ group grafted was 1.6106 mmol/g .

- $MCS-NH_2$ showed high adsorption capacities for Pb^{2+} , Cd^{2+} , Cr^{3+} , and Cu^{2+} at pH 5.0–7.5 in the following order: Pb^{2+} (717.97 mg/g) > Cd^{2+} (631.43 mg/g) > Cu^{2+} (628.61 mg/g) > Cr^{3+} (366.88 mg/g) (293 K). These values are much higher than those reported in literature. The equilibrium data of the four heavy metal ions adsorbed by $MCS-NH_2$ fitted the Langmuir and Redlich-Peterson models well, but the latter was more suitable than the former. The adsorption processes of the four heavy metal ions were all endothermic, entropy increasing, and spontaneous. The adsorptions of $MCS-NH_2$ for Pb^{2+} , Cd^{2+} , Cr^{3+} , and Cu^{2+} were all rapid and reached equilibrium within 60 min. The adsorption kinetics could be fitted well by the pseudo second-order model, and the order of adsorption activation energy was Cr^{3+} (25.9062 kJ/mol) > Pb^{2+} (21.0187 kJ/mol) > Cd^{2+} (18.1051 kJ/mol) > Cu^{2+} (16.8084 kJ/mol).
- $MCS-NH_2$ adsorbed with heavy metals could be regenerated by 0.1 mol/L of triethylene tetramine. The adsorption mechanisms included physical adsorption, chemical adsorption (especially surface complexing adsorption), and ion exchange. Chemical adsorption was the dominant mechanism. $MCS-NH_2$ exhibited excellent adsorption of Pb^{2+} , Cd^{2+} , Cr^{3+} , and Cu^{2+} and is thus a promising adsorption material with excellent properties for heavy metal ions.

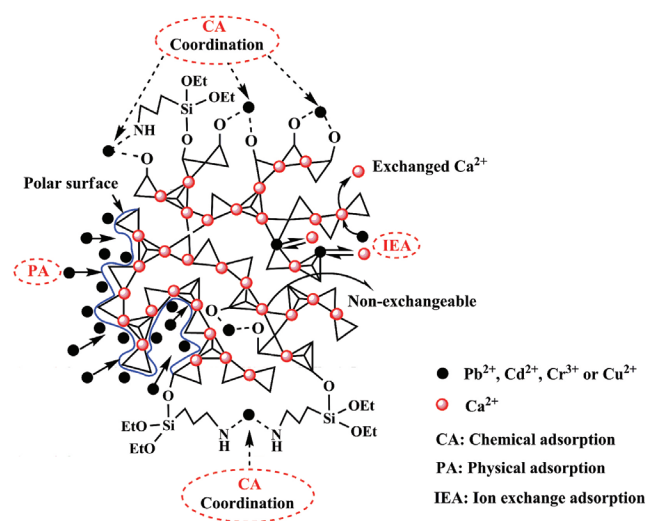


Fig. 13. Proposed adsorption mechanism.

Acknowledgments

This research was supported by the National Nature Science Foundation of China (Grant No. 51378201) and the Scientific Research Fund of Hunan Education Department (Grant No. 16A069).

References

- X.Y. Guo, B. Du, Q. Wei, J. Yang, L.H. Hu, L.H. Yan, W.Y. Xu, Synthesis of amino functionalized magnetic graphenes composite material and its application to remove Cr (VI), Pb (II), Hg (II), Cd (II) and Ni (II) from contaminated water, *J. Hazard. Mater.*, 278 (2014) 211–220.
- I. Giannopoulou, D. Panians, Differential precipitation of copper and nickel from acidic polymetallic aqueous solutions, *Hydrometallurgy*, 90 (2008) 137–146.
- L.H. Liu, J. Wu, X. Li, Y.L. Ling, Synthesis of poly (dimethyldiallylammonium chloride-co-acrylamide)-graft-triethylenetetramine-dithiocarbamate and its removal performance and mechanism of action towards heavy metal ions, *Sep. Purif. Technol.*, 103 (2013) 92–100.

- [4] T.P. Phetla, F. Ntuli, E. Muzenda, Reduction crystallization of Ni, Cu, Fe and Co from a mixed metal effluent, *J. Ind. Eng. Chem.*, 18 (2012) 1171–1177.
- [5] Y.J. Tu, C.K. Chang, C.F. Youa, S.L. Wang, Treatment of complex heavy metal wastewater using a multi-staged ferrite process, *J. Hazard. Mater.*, 209–210 (2012) 379–384.
- [6] C.W. Wong, J.P. Barford, G. Chen, G. McKay, Kinetics and equilibrium studies for the removal of cadmium ions by ion exchange Resin, *J. Environ. Chem. Eng.*, 2 (2014) 698–707.
- [7] J.H. Huang, F. Yuan, G.M. Zeng, X. Li, Y.L. Gu, L. Shi, W. Liu, Y.X. Shi, W.C. Liu, Y.H. Shi, Influence of pH on heavy metal speciation and removal from wastewater using micellar-enhanced ultrafiltration, *Chemosphere*, 173 (2017) 199–206.
- [8] Y.F. Huang, D.H. Wu, X.D. Wang, W. Huang, D. Lawless, X.S. Feng, Removal of heavy metals from water using polyvinylamine by polymer-enhanced ultrafiltration and flocculation, *Sep. Purif. Technol.*, 158 (2016) 124–136.
- [9] J.E.D.V. Segundo, G.R. Salazar-Banda, A.C.O. Feitoza, E.O. Vilar, E.B. Cavalcanti, Cadmium and lead removal from aqueous synthetic wastes utilizing Chemelec electrochemical reactor: Study of the operating conditions, *Sep. Purif. Technol.*, 88 (2012) 107–115.
- [10] T.K. Tran, K.F. Chiu, C.Y. Lin, H.J. Leu, Electrochemical treatment of wastewater: Selectivity of the heavy metals removal process, *Int. J. Hydrogen Energy*, (2017) 1–8, (in press).
- [11] M. Taseidifar, F. Makavipour, R.M. Pashley, A.F.M.M. Rahman, Removal of heavy metal ions from water using ion flotation, *Environ. Technol. Innov.*, 8 (2017) 182–190.
- [12] I. Abdelfattaha, A.A. Ismail, F.A. Sayedc, A. Almedolab, K.M. Aboelghait, Biosorption of heavy metals ions in real industrial wastewater using peanut husk as efficient and cost effective adsorbent, *Environ. Nanotechnol. Monit. Manage.*, 6 (2016) 176–183.
- [13] M. Kumari, C.U. Pittman Jr, D. Mohan, Heavy metals [chromium (VI) and lead (II)] removal from water using mesoporous magnetite (Fe₃O₄) nanospheres, *J. Colloid Interface Sci.*, 442 (2015) 120–132.
- [14] H.P. Zhang, L.Q. Gu, L. Zhang, S.R. Zheng, H.Q. Wan, J.Y. Sun, D.Q. Zhu, Z.Y. Xu, Removal of aqueous Pb (II) by adsorption on Al₂O₃-pillared layered MnO₂, *Appl. Surf. Sci.*, 406 (2017) 330–338.
- [15] M. Prica, S. Adamovic, B. Dalmacija, L. Rajic, J. Trickovic, S. Rapajic, M. Becelic-Tomin, The electrocoagulation/flotation study: Theremoval of heavy metals from the waste fountain solution, *Process Saf. Environ. Prot.*, 94 (2015) 262–273.
- [16] F.L. Fu, Q. Wang, Removal of heavy metal ions from wastewaters: A review, *J. Environ. Manage.*, 92 (2011) 407–418.
- [17] A. Sheikh Hosseini, M. Shirvani, H. Shariatmadari, Competitive sorption of nickel, cadmium, zinc and copper on palygorskite and sepiolite silicate clay minerals, *Geoderma*, 192 (2013) 249–253.
- [18] A. Sdiri, M. Khairy, S. Bouaziz, S. El-Safty, A natural clayey adsorbent for selective removal of lead from aqueous solutions, *Appl. Clay Sci.*, 126 (2016) 89–97.
- [19] L. Largette, J. Laminie, Modelling the lead concentration decay in the adsorption of lead onto a granular activated carbon, *J. Environ. Chem. Eng.*, 3 (2015) 474–481.
- [20] W.J. Peng, H.Q. Li, Y.Y. Liu, S.X. Song, A review on heavy metal ions adsorption from water by graphene oxide and its composites, *J. Mol. Liq.*, 230 (2017) 496–504.
- [21] C. Chen, H.B. Liu, T.H. Chen, D. Chen, R.L. Frost, An insight into the removal of Pb (II), Cu (II), Co (II), Cd (II), Zn (II), Ag (I), Hg (I), Cr (VI) by Na (I)-montmorillonite and Ca (II)-montmorillonite, *Appl. Clay Sci.*, 118 (2015) 239–247.
- [22] U. Habiba, A.M. Afifi, A. Salleh, B.C. Ang, Chitosan/(polyvinyl alcohol)/zeolite electrospun composite nanofibrous membrane for adsorption of Cr⁶⁺, Fe³⁺ and Ni²⁺, *J. Hazard. Mater.*, 322 (2017) 182–194.
- [23] B. Hayati, A. Maleki, F. Najafi, H. Daraei, F. Gharibi, G. McKay, Synthesis and characterization of PAMAM/CNT nanocomposite as a super-capacity adsorbent for heavy metal (Ni²⁺, Zn²⁺, As³⁺, Co²⁺) removal from wastewater, *J. Mol. Liq.*, 224 (2016) 1032–1040.
- [24] F. Ke, J. Jiang, Y.Z. Li, J. Liang, X.C. Wan, S. Ko, Highly selective removal of Hg²⁺ and Pb²⁺ by thiol-functionalized Fe₃O₄@metal-organic framework core-shell magnetic microspheres, *Appl. Surf. Sci.*, 413 (2017) 266–274.
- [25] M. Anbia, M. Haqshenas, Adsorption studies of Pb(II) and Cu(II) ions on mesoporous carbon nitride functionalized with melamine-based dendrimer amine, *Int. J. Environ. Sci. Technol.*, 12 (2015) 2649–2664.
- [26] M. Shafiabadi, A. Dashti, H.A. Tayebi, Removal of Hg (II) from aqueous solution using polypyrrole/SBA-15 nanocomposite: Experimental and modeling, *Synth. Met.*, 212 (2016) 154–160.
- [27] M. Anbia, K. Kargosha, S. Khoshbouei, Heavy metal ions removal from aqueous media by modified magnetic mesoporous silica MCM-48, *Chem. Eng. Res. Des.*, 93 (2015) 779–788.
- [28] L.C. Lin, M. Thirumavalavan, J.F. Lee, Facile synthesis of thiol-functionalized mesoporous silica-their role for heavy metal removal efficiency, *Clean-Soil, Air, Water*, 43(5) (2015) 775–785.
- [29] Y.J. Jia, Y.J. Zhang, R.W. Wang, J.J. Yi, X. Feng, Q.H. Xu, Mesoporous zirconium phosphonate hybrid material as adsorbent to heavy metal ions, *Ind. Eng. Chem. Res.*, 51(38) (2012) 12266–12273.
- [30] T.Y. Ma, X.J. Zhang, G.S. Shao, A.J.L. Cao, Z.Y. Yuan, Ordered Macroporous titanium phosphonate materials: Synthesis, photocatalytic activity, and heavy metal ion adsorption, *J. Phys. Chem. C*, 112(8) (2008) 3090–3096.
- [31] Z.X. Wu, P.A. Webley, D.Y. Zhao, Comprehensive study of pore evolution, mesostructural stability, and simultaneous surface functionalization of ordered mesoporous carbon (FDU-15) by wet oxidation as a promising adsorbent, *Langmuir*, 26(12) (2010) 10277–10286.
- [32] I. Maruyama, G. Igarashi, Y. Nishioka, Bimodal behavior of C-S-H interpreted from short-term length change and water vapor sorption isotherms of hardened cement paste, *Cem. Concr. Res.*, 73 (2015) 158–168.
- [33] P. Duan, Z.H. Shui, W. Chen, C.H. Shen, Influence of super plasticizer on composition and pore structure of C-S-H, *Constr. Build. Mater.*, 44 (2013) 87–91.
- [34] D.A. Kulik, Improving the structural consistency of C-S-H solid solution thermodynamic models, *Cem. Concr. Res.*, 41 (2011) 477–495.
- [35] M.Y. Shie, H.C. Chang, S.J. Ding, Composition-dependent protein secretion and integrin level of osteoblastic cell on calcium silicate cements, *J. Biomed. Mater. Res. Part A*, 102A (2014) 769–780.
- [36] C.C. Chen, C.C. Ho, S.Y. Lin, S.J. Ding, Green synthesis of calcium silicate bioceramic powders, *Ceram. Int.*, 41 (2015) 5445–5453.
- [37] F.S. Shirazi, M. Mehrali, A.A. Oshkour, H.S.C. Metselaar, N.A. Kardi, N.A. Abu Osman, Mechanical and physical properties of calcium silicate/alumina composite for biomedical engineering applications, *J. Mech. Behav. Biomed. Mater.*, 30 (2014) 168–175.
- [38] B.H. Kan, L.Z. Feng, K.Y. Zhao, J.F. Wei, D.W. Zhu, L.H. Zhang, Q. Ren, Preparation and rebinding properties of protein imprinted polysiloxane using mesoporous calcium silicate grafted non-woven polypropylene as matrix, *J. Mol. Recognit.*, 29(3) (2016) 115–122.
- [39] K. Okano, M. Uemoto, J. Kagami, K. Miura, T. Aketo, M. Toda, K. Honda, H. Ohtake, Novel technique for phosphorus recovery from aqueous solutions using amorphous calcium silicate hydrates (A-CSHs), *Water Res.*, 47 (2013) 2251–2259.
- [40] K.Y. Zhao, T. Chen, D.Y. Li, X.X. Zhang, J.F. Wei, H.Y. Song, Preparation and characterization of mesoporous calcium silicate grafted polypropylene non-woven fabric, *Mater. Lett.*, 141 (2015) 110–113.
- [41] K. Okano, S. Miyamaru, A. Kitao, H. Takano, T. Aketo, M. Toda, K. Honda, H. Ohtake, Amorphous calcium silicate hydrates and their possible mechanism for recovering phosphate from wastewater, *Sep. Purif. Technol.*, 144 (2015) 63–69.
- [42] W. Guan, F.Y. Jin, Q.K. Chen, P. Yan, Q. Zhang, Preparation and phosphorus recovery performance of porous calcium-silicate-hydrate, *Ceram. Int.*, 39 (2013) 1385–1391.
- [43] C.J. Li, M.H. Wan, Y. Dong, Z.Y. Men, Y. Lin, D.Y. Wu, H.N. Kong, Treating surface water with low nutrients concentra-

- tion by mixed substrates constructed wetlands, *J. Environ. Sci. Health Part A.*, 46 (2011) 771–776.
- [44] X.H. Wang, K.Y. Zhao, B.X. Yang, T. Chen, D.Y. Li, H. Wu, J.F. Wei, X.Q. Wu, Adsorption of Dibutyl phthalate in aqueous solution by mesoporous calcium silicate grafted non-woven polypropylene, *Chem. Eng. J.*, 306 (2016) 452–459.
- [45] W. Guan, X. Zhao, Fluoride recovery using porous calcium silicate hydrates via spontaneous Ca^{2+} and OH^- release, *Sep. Purif. Technol.*, 165 (2016) 71–77.
- [46] K.Y. Zhao, X.H. Wang, T. Chen, H. Wu, J.G. Li, B.X. Yang, D.Y. Li, J.F. Wei, Bisphenol A adsorption properties of mesoporous $\text{CaSiO}_3@SiO_2$ grafted non-woven polypropylene fiber, *Ind. Eng. Chem. Res.*, 56 (2017) 2549–2556.
- [47] G.X. Qi, X.F. Lei, L. Li, C. Yuan, Y.L. Sun, J.B. Chen, J. Chen, Y. Wang, J.M. Hao, Preparation and evaluation of a mesoporous calcium-silicate material (MCSM) from coal fly ash for removal of Co (II) from wastewater, *Chem. Eng. J.*, 279 (2015) 777–787.
- [48] J. Wu, Y.J. Zhu, F. Chen, Ultrathin calcium silicate hydrate nanosheets with large specific surface areas: synthesis, crystallization, layered self-assembly and applications as excellent adsorbents for drug, protein, and metal ions, *Small*, 9(17) (2013) 2911–2925.
- [49] J. Zhao, Y.J. Zhu, J. Wu, J.Q. Zheng, X.Y. Zhao, B.Q. Lu, F. Chen, Chitosan-coated mesoporous microspheres of calcium silicate hydrate: Environmentally friendly synthesis and application as a highly efficient adsorbent for heavy metal ions, *J. Colloid Interface Sci.*, 418 (2014) 208–215.
- [50] S. Shaw, S.M. Clark, C.M.B. Henderson, Hydrothermal formation of the calcium silicate hydrates, tobermorite ($\text{Ca}_5\text{Si}_6\text{O}_{16}(\text{OH})_2 \cdot 4\text{H}_2\text{O}$) and xonotlite ($\text{Ca}_3\text{Si}_2\text{O}_7(\text{OH})_2$): An in situ synchrotron study, *Chem. Geol.*, 167 (2000) 129–140.
- [51] M.L. Zhang, J. Chang, Surfactant-assisted sonochemical synthesis of hollow calcium silicate (CSH) microspheres for drug deliver, *Ultrason. Sonochem.*, 17(5) (2010) 789–792.
- [52] N.Y. Mostafa, E.A. Kishar, S.A. Abo-El-Enein, FTIR study and cation exchange capacity of Fe^{3+} - and Mg^{2+} -substituted calcium silicate hydrates, *J. Alloys Compd.*, 473 (2009) 538–542.
- [53] Q. Li, J.G. Yu, F. Zhou, X.Y. Jiang, Synthesis and characterization of dithiocarbamate carbon nanotubes for the removal of heavy metal ions from aqueous solutions, *Colloids Surf. A: Physicochem. Eng. Aspects*, 482 (2015) 306–314.
- [54] K.M.M. Aguilar, Y. Amano, M. Machida, Ammonium persulfate oxidized activated carbon fibers: Analysis of their oxidation debris quantity and their useful for aqueous Pb (II) batch and column experiments, *J. Fiber Sci. Technol.*, 73(7) (2017) 150–157.
- [55] P. Tan, Y.Y. Hu, Q. Bi, Competitive adsorption of Cu^{2+} , Cd^{2+} and Ni^{2+} from an aqueous solution on graphene oxide membranes, *Colloids Surf. A: Physicochem. Eng. Aspects*, 509 (2016) 56–64.
- [56] X.Y. Li, H.H. Zhou, W.Q. Wu, S.D. Wei, Y. Xu, Y.F. Kuang, Studies of heavy metal ion adsorption on Chitosan/Sulfhydryl functionalized graphene oxide composites, *J. Colloid Interface Sci.*, 448 (2015) 389–397.
- [57] N. Torapava, A. Radkevich, D. Davydov, A. Titov, I. Persson, Composition and Structure of Polynuclear Chromium (III) Hydroxo Complexes, *Inorg. Chem.*, 48 (2009) 10383–10388.
- [58] J. Tits, E. Wieland, C.J. Müller, C. Landesman, M.H. Bradbury, Strontium binding by calcium silicate hydrates, *J. Colloid Interface Sci.*, 300 (2006) 78–87.

Supplementary data

Particle size distributions of MCS-NH₂ and MCS

For the determination procedure, the synthesized MCS-NH₂ and MCS were sieved through 400 mesh sieves after grinding for 1 h. The particle size distributions of MCS-NH₂ and MCS in water were determined through NSKC-1A Centrifugal Light Transmission Granulometry (Nanjing University of Chemical Technology, China). The particle size distributions of MCS-NH₂ and MCS in water are shown in Table A.1.

Adsorption isotherm models

The relationship between an adsorbent and adsorbate is described by adsorption isotherms, and the isothermal adsorption data usually employ the Langmuir model [Eq. (A.1)], Freundlich model [Eq. (A.2)], and Redlich–Peterson model [Eq. (A.3)] [1]. In this work, the three models were employed to fit the adsorption experimental data and obtain the thermodynamic parameters.

$$q_e = \frac{Qb c_e}{1 + b c_e} \quad (\text{A.1})$$

$$q_e = K_F c_e^n \quad (\text{A.2})$$

$$q_e = \frac{K_{R-P} c_e}{1 + \alpha c_e^\beta} \quad (\text{A.3})$$

where q_e is the amount of adsorbed heavy metal ion per weight unit of MCS-NH₂ at equilibrium (mg/g); b is a constant related to the affinity of the binding sites (L/mg); Q is the maximum amount of heavy metal ion per weight unit of MCS-NH₂ (mg/g); c_e is the concentration of heavy metal ion in solution at equilibrium (mg/L); K_F is the Freundlich constant; n is a constant, usually exceeds 1; and K_{R-P} , α , and β are the Redlich–Peterson constants, where β lies between 0 and 1.

Adsorption thermodynamic parameters

The logarithmic function $\ln K_d$ of the distribution coefficient K_d [Eq. (A.4)] was plotted against the reciprocal of temperature $1/T$. By linear fitting, the enthalpy change ΔH and entropy change ΔS of the adsorption process were obtained from the linear slope and intercept, respectively [Eq. (A.5)].

Then, the Gibbs free energy of ΔG was calculated through Eq. (A.6) and indicated the adsorption reaction type and reaction degree.

$$K_d = \frac{x/m}{y/v} \quad (\text{A.4})$$

$$\ln K_d = \frac{\Delta S}{R} - \frac{\Delta H}{RT} \quad (\text{A.5})$$

$$\Delta G = \Delta H - T\Delta S \quad (\text{A.6})$$

where x and y are the masses (mg) of heavy adsorbed and in solution, respectively; m is the mass of the adsorbent in g; and v is the volume of the solution in mL. Therefore, x/m and y/v are the solid-phase concentration q_e (mg/g) and the equilibrium concentration in solution c_e (mg/L) at equilibrium, respectively.

Adsorption kinetic models and adsorption activation energy

The equation for the pseudo-first-order kinetic model is given as follows:

$$q_t = q_e(1 - e^{-k_1 t}) \quad (\text{A.7})$$

where q_t (mmol/g) is the amount of heavy metal ion adsorbed per unit mass of adsorbent at time (t); q_e (mmol/g) is the amount of heavy metal ion adsorbed per unit mass of adsorbent at equilibrium; and k_1 (min⁻¹) is the pseudo-first-order kinetic constant.

By contrast, the pseudo-second-order kinetic model is represented by the following:

$$q_t = \frac{k_2 q_e^2 t}{1 + k_2 q_e t} \quad (\text{A.8})$$

where q_t (mmol/g) is the amount of heavy metal ion adsorbed per unit mass of adsorbent at time (t); q_e (mmol/g) is the amount of heavy metal ion adsorbed per unit mass of adsorbent at equilibrium; and k_2 (g/mmol·min) is the pseudo-second-order kinetic constant.

The logarithm of the adsorption rate constant ($\ln k$) can be calculated, and the curve of the variation of the adsorption rate constant with temperature was obtained by plotting $\ln k$ against the reciprocal of temperature $1/T$.

Table A.1
Particle size distribution of MCS-NH₂ and MCS in water

Sample	Mass fraction (%)											
	0–1 (μm)	1–2 (μm)	2–3 (μm)	3–4 (μm)	4–5 (μm)	5–6 (μm)	6–7 (μm)	7–8 (μm)	8–10 (μm)	10–15 (μm)	15–20 (μm)	20–45 (μm)
MCS-NH ₂	1.10	5.21	5.62	6.52	7.21	8.32	9.51	16.16	15.33	15.04	8.83	1.15
MCS	2.85	4.98	5.85	6.12	6.25	6.90	11.37	15.25	17.53	12.64	6.94	3.32

Table A.2
Energy spectrum analysis results of MCS-NH₂ (a) and MCS (b)

Element	(a) MCS-NH ₂		(b) MCS	
	Mass percent (%)	Atomic number percent (%)	Mass percent (%)	Atomic number percent (%)
O	28.325	31.240	51.813	67.790
Si	26.756	16.810	31.575	23.534
Ca	13.245	5.831	16.612	8.675
N	1.988	2.505		
C	29.684	43.611		

Table A.3
pH values of simulated heavy metal solutions

Metal ion	pH					
	25 mg/L	50 mg/L	75 mg/L	100 mg/L	125 mg/L	150 mg/L
Pb ²⁺	5.79	5.70	5.59	5.51	5.43	5.39
Cd ²⁺	6.51	6.45	6.37	6.17	6.05	6.02
Cr ³⁺	5.24	5.35	5.15	5.24	5.27	5.32
Cu ²⁺	5.83	5.72	5.57	5.48	5.41	5.42

The curve can then be fitted by linear regression, and the adsorption activation energy (E_a) can be calculated from the slope of the regression line in accordance with the

Table A.4
Nonlinear fitting parameters of MCS-NH₂ for Pb²⁺, Cd²⁺, Cr³⁺ and Cu²⁺

Metal ion	T (K)	Langmuir			Freundlich			Redlich-Peterson			
		Q (mg/g)	b (L/mg)	R^2	K_F	n	R^2	K_{R-P}	α	β	R^2
Pb ²⁺	293	717.97	1.8026	0.9863	399.36	3.7613	0.8980	1738.19	2.8655	0.9212	0.9938
	303	717.88	2.3118	0.9950	419.51	3.9018	0.8550	1771.72	2.5791	0.9760	0.9919
	313	734.69	2.0392	0.9963	421.16	3.7755	0.8665	1623.58	2.3261	0.9713	0.9962
	323	744.78	2.5948	0.9933	452.63	4.0602	0.8074	1777.63	2.2554	1.0307	0.9931
Cd ²⁺	293	631.43	1.7828	0.9740	349.26	4.3387	0.9068	1784.58	3.5811	0.9043	0.9985
	303	650.76	1.9993	0.9889	367.79	4.4541	0.8754	1699.97	3.0357	0.9379	0.9987
	313	659.40	2.5763	0.9952	388.84	4.7122	0.8384	1891.06	3.0592	0.9719	0.9967
	323	683.89	2.9901	0.9956	413.05	4.9174	0.7792	1980.82	2.8372	1.0093	0.9945
Cr ³⁺	293	366.88	0.1809	0.9722	116.16	3.7702	0.9605	118.63	0.5740	0.8660	0.9961
	303	392.53	0.1885	0.9871	126.87	3.8146	0.9232	94.03	0.3190	0.9324	0.9896
	313	405.46	0.2301	0.9837	144.00	4.1046	0.8663	91.40	0.2194	1.0065	0.9783
	323	422.99	0.2823	0.9697	162.16	4.3578	0.8101	99.35	0.1804	1.0652	0.9668
Cu ²⁺	293	628.61	1.5544	0.9829	337.90	4.4467	0.8892	1373.62	2.6630	0.9259	0.9951
	303	642.39	2.2225	0.9958	369.14	4.7812	0.8339	1611.16	2.7064	0.9689	0.9986
	313	663.19	2.2080	0.9969	385.94	4.8294	0.7839	1405.52	2.0448	1.0087	0.9987
	323	674.91	3.1650	0.9869	415.42	5.1289	0.7484	2062.40	2.9734	1.0066	0.9835

Arrhenius equation [Eq. (A.9)]. The adsorption type can be determined further.

$$\ln k = -\frac{E_a}{RT} + B \quad (\text{A.9})$$

where k is the adsorption rate constant; R is the molar gas constant 8.314 J/mol·K; T is the absolute temperature (K); E_a is the activation energy of adsorption in kJ/mol; and B is the constant.

References

- [1] O. Redlich, D.L. Peterson, A useful adsorption isotherm, *J. Phy. Chem.*, 63(6) (1959) 1024.
- [2] D. Ghosh, K.G. Bhattacharyya, Adsorption of methylene blue on kaolinite, *Appl. Clay Sci.*, 20 (2002) 295–300.

Table A.5
Kinetic fitting parameters

Metal ion	T (K)	Pseudo-first-order kinetics model			Pseudo-second-order kinetics model			Experimental value q_{ed} (mmol/g)
		q_e (mmol/g)	k_1 (min ⁻¹)	R^2	q_e (mmol/g)	k_2 (g/mmole·min)	R^2	
Pb ²⁺	293	3.4518	1.8556	0.6629	3.4652	4.9891	0.9730	3.3747
	303	3.4891	1.9539	0.6527	3.5004	5.9372	0.9411	3.3891
	313	3.5387	2.1027	0.6527	3.5471	8.0538	0.9513	3.4167
	323	3.5888	2.2629	0.6474	3.5949	11.0169	0.9346	3.4015
Cd ²⁺	293	5.5639	1.3637	0.6579	5.6203	1.1284	0.9648	5.7628
	303	5.7382	1.4778	0.7301	5.7815	1.4605	0.9617	5.8393
	313	5.8361	1.6273	0.6904	5.8704	1.8909	0.9722	5.9043
	323	5.9591	1.7861	0.4856	5.9902	2.2252	0.9376	5.9834
Cr ³⁺	293	6.5752	0.4695	0.8408	6.8807	0.1328	0.9947	6.7634
	303	6.9694	0.5577	0.7865	7.2464	0.1612	0.9867	7.2292
	313	7.1428	0.7652	0.7584	7.3510	0.2524	0.9912	7.4146
	323	7.5850	0.9348	0.7355	7.7488	0.3465	0.9898	7.7452
Cu ²⁺	293	9.8730	2.2046	0.6215	9.8925	3.4764	0.9453	10.0659
	303	10.0909	2.3286	0.4262	10.1087	3.9681	0.9194	10.1635
	313	10.3357	2.4117	0.5396	10.3494	4.9973	0.9406	10.3154
	323	10.6106	2.5440	0.6734	10.6209	6.5836	0.9619	10.5305

Table A.6
Activation energy of MCS-NH₂ adsorption with Pb²⁺, Cd²⁺, Cr³⁺ and Cu²⁺

Metal ion	Pb ²⁺	Cd ²⁺	Cr ³⁺	Cu ²⁺
Activation energy Ea (kJ/mol)	21.0187	18.1051	25.9062	16.8084